ADVANCED METHODS OF CHARACTERISATION OF THE THIN CHALCOGENIDE FILMS, PASSIVE AND ACTIVE OPTICAL WAVEGUIDES

Simona DONŢU [1], Aurelian A. POPESCU[2], Dan SAVASTRU[3], Vasile SAVA [4], Bogdan CHIRICUŢĂ[5], Mona MIHĂILESCU[6], Constantin NEGUŢU[7], Georgiana C. VASILE[8] and Niculae N. PUŞCAŞ[9]

În acest articol prezentăm o recenzie privind câteva rezultate experimentale în care se utiliează metode optice nedistructive pentru caracterizarea filmelor subţiri din sticle semiconductoare calcogenice şi a ghidurilor optice de undă de tip Er^{3+}:Ti:LiNbO₃ ca: atenuarea luminii, distribuţia spaţială a indicelui de refracţie, dispersia indicelui de refracţie, spectre de emisie si absorbţie care se datorează elementelor pământurilor rare. Metoda rezonatorului optic şi metoda cuplajului cu prismă sunt potrivite pentru măsurarea atenuării în ghidurile planare întrucât depind de structura specifică a acestora. Metoda celor trei prisme poate fi utilizată pentru caracterizarea ghidurilor optice planare cu pierderi optice mici. Ghidurile optice planare cu pierderi optice mici pot fi realizate utilizând structuri calcogenice multistrat de tip As_xS_{1-x} cu diferite compoziţii. Profilul indicelui de refracţie poate fi determinat din măsurători de câmp apropiat, sau cu tehnici holografice sau cu tehnici spectroscopice de tip "m-line". Anizotropia indicelui de refracţie poate fi de ordinul 0.02 în filme amorfe subţiri. În cazul măsurătorilor dispersiei indicelui de refracţie în cazul ghidurilor de tip As_2S_3 s-a obţinut valoarea maximă în domeniul lungimilor de undă 0.80µm - 0.85µm.

In this paper we report a review concerning some experimental results using non-destructive optical methods for the characterization of the thin films of semiconductor chalcogenide glasses and Er^{3+}- doped Ti:LiNbO₃ waveguides,

---

[1] National Institute R&D of Optoelectronics, INOE 2000, 409 Atomistilor str., PO BOX MG. 5, 77125 Magurele, Ilfov, Romania.

[2] National Institute R&D of Optoelectronics, INOE 2000, 409 Atomistilor str., PO BOX MG. 5, 77125 Magurele, Ilfov, Romania

[3] National Institute R&D of Optoelectronics, INOE 2000, 409 Atomistilor str., PO BOX MG. 5, 77125 Magurele, Ilfov, Romania

[4] S.C. Apel Laser SRL, Vintila Mihailescu Str., No. 15, Bl. 60, Sc. 1, Et. 1, Ap. 12, Sect. 6, Bucharest, Romania.

[5] .C. Apel Laser SRL, Vintila Mihailescu Str., No. 15, Bl. 60, Sc. 1, Et. 1, Ap. 12, Sect. 6, Bucharest, Romania

[6] Lecturer, Physics Department, University POLITEHNICA of Bucharest, Romania

[7] Lecturer, Physics Department, University POLITEHNICA of Bucharest, Romania

[8] Assist., Physics Department, University POLITEHNICA of Bucharest, Romania

[9] Prof., Physics Department, University POLITEHNICA of Bucharest, Romania, email: pnt@physics.pub.ro

such as: light attenuation in planar, refractive index spatial distribution, dispersion of refractive index, absorption and emission spectra which is due to rare earth elements. Depending on the specific structure, resonator method or prism coupling method are favorable for the attenuation measurements in planar waveguides. A three prism method can be used for the characterisation of planar waveguides with low optical losses. The low loss planar waveguides can be realised using a multilayer structure of As_xS_{1-x} chalcogenide films with different compositions. The refractive index profile can be established from near field measurements, by using holographic technique or m-line spectroscopy. The refractive index anisotropy can reach the level of 0,02 in thin amorphous films. The measurements of the refractive index dispersion curve of the As_2S_3 waveguides have found a maximum that occur for the wavelength range between 0.80μm and 0.85μm.

Keywords: optical waveguides, chalcogenide glasses, optical losses, refractive index profile, refractive index dispersion.

1. Introduction

In the recent years many passive and active devices have been realized in $LiNbO_3$ crystal due to its good electro optical, acousto-optic and nonlinear properties and its use in compact and efficient integrated devices such as: amplitude and phase modulator, tunable filters, directional couplers, lasers and amplifiers and switches for signal processing, it is then extremely important to experimentally characterize the emission, absorption and guiding properties of Er^{3+}-doped Ti:$LiNbO_3$ waveguides using non-destructive methods [1-6].

For the developments of hybrid integrated optics, besides lithium niobate silicon (in SOI concept), Ga-Al-As are known as priority candidates. The As_xS_{1-x} vitreous chalcogenide semiconductors have a number of favorable properties, namely: a refractive index higher than two that is required for manufacturing of photonic crystals [7, 8]; the refractive index may vary within a large range (2.0 – 2.8) that is required for the manufacturing the light confinement structures [9]; a considerable value of the Kerr nonlinearity constant [10,11] of about 10^2-10^3 times higher than the quartz. From several papers it follows that the chalcogenide planar waveguides have usually optical losses about 3-5 dB/cm and the main cause for the losses is the scattering of the light, caused by the poor substrate quality, the surface roughness and others.

In Sec. 2 we present some results concerning the evaluation of the attenuation coefficient from the measured transmitted signal and experimental investigations of the optical losses in planar waveguides and manufacture of planar multilayer waveguides with low losses, respectively.

Sec. 3 is devoted to the refractive index profile reconstruction from deconvoluted near field measurement, to the refractive index profile obtained

using holographic investigations and refractive index anisotropy in As_2S_3 films and dispersion of the refractive index in As_2S_3 films.

In Sec. 4 the theoretical model for Stark splitted Er ions has been used for cross section calculation assuming the absorption spectra starting point. In Sec. 5 we present our conclusions concerning the obtained results.

2. Evaluation of the attenuation coefficients

2.1. Measurement of losses using resonator method

The waveguide propagation losses α may be evaluated through the measurement of transmitted light intensity, I_T considering the guide as a low-finesse optical resonator using the equation [6,12]:

$$I_T = \frac{T^2 \exp(-\alpha L)}{(1-\widetilde{R})^2 + 4\widetilde{R}\sin^2(\Phi/2)} I_0 \eta \tag{1}$$

where I_0 is the incident intensity, η is the coupling efficiency between the incident laser beam and the waveguide mode profile, T represents the end face mode transmissivity, L the waveguide length, phase difference and $\widetilde{R}$ is defined as: $\widetilde{R} = R\exp(-\alpha L)$.

The variation of the optical transmission may be used to make a relative measurement to determine the resonance contrast K defined between two limits, an upper value, I_M and a lower value, I_m as:

$$K = \frac{I_M - I_m}{I_M + I_m}. \tag{2}$$

By using Eq. (2) the coefficient K may be evaluated experimentally, and from Eq. (1) as a function of $\widetilde{R}$ independently from the other parameters yielding the following equation for the attenuation coefficient:

$$\alpha \sim \frac{4.34}{L}(\ln R + \ln 2 - \ln\widetilde{K}) \tag{3}$$

An estimation of the absolute error of the attenuation coefficient may be computed by differentiating Eq. (3) using:

$$\Delta\alpha = \frac{4.34}{L}\frac{|\Delta K|}{K} \tag{4}$$

showing that the absolute error in the calculation of α depends on the relative error in the contrast measurement.

The experimental setup used to measure the attenuation coefficient with the resonator method is shown schematically in Fig. 1. We used a He-Ne laser

(λ=0.63 μm) for alignment and a laser diode (L. D.) at λ=1.55 μm for the optical signal, coupled together by a 3 dB coupler (C). The losses of some Er^{3+} :Ti:LiNbO$_3$ and Ti:LiNbO$_3$ optical strip waveguides (W) X-cut 48 mm long and Z-cut 52 mm long have been evaluated. The waveguides widths range from 5μm to 9 μm. The resonator method proved to be especially suitable for evaluating the total loss of both polarizations.

The output signal from the waveguides has been detected by an optical spectrum analyser (O. S. A.) used like a photodiode; then the measured data have been acquired by a computer (CO.). By measuring the contrast of the Fabry-Pérot resonances (Fig. 2) it is possible to evaluate a combined loss-reflection factor and thus give an estimation of the upper limit for the attenuation coefficient. In Eq. (1) the transmitted intensity varies periodically with the phase difference and may be tuned varying the temperature of the waveguide using a heating Peltier element (O).
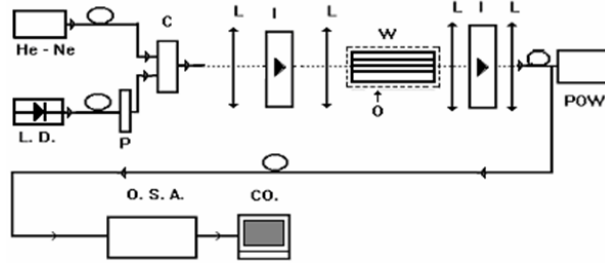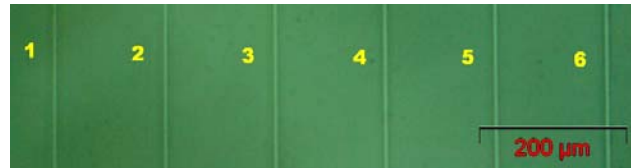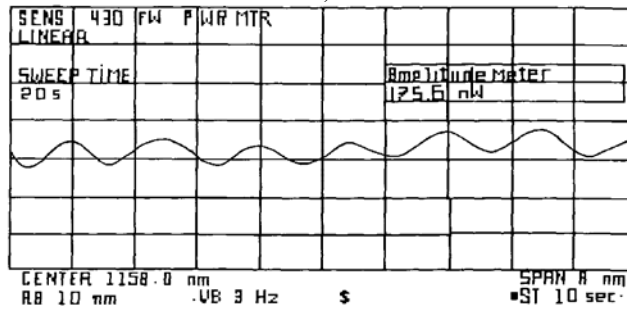

Fig. 1. Schematically experimental set-up for the attenuation coefficient measurement.

a)

b)

Fig. 2. a**)** A SEM image for X-cut optical waveguides and **b)** the corresponding transmitted intensity for waveguide 5 of 7.5 μm wide.

The measurement of the emergent light from the waveguide was performed using a standard optical fibre (see Fig. 2a) for the SEM image of the waveguides and Fig. 2b for number 5 corresponding to the transmitted intensity directly coupled with a powermeter (POW.). The displacement of the optical fibre mounted on a support was obtained with an electrostrictive actuator controller (E. A. C.) interfaced with computer to register the waveguide field intensity profile in depth and width for TE and TM polarizations selected by the polarization controller (P) and the isolator (I). By measuring the contrast of the Fabry-Pérot resonances for example in the case of a 7.5 µm wide X-cut waveguide (the waveguide number 5 from Fig. 2 a) it is possible to evaluate a combined loss reflection and thus give an upper limit estimation for the attenuation coefficient [6,13].

In Fig. 3 we present some values of the attenuation coefficient in the case of X-cut Er^{3+}:Ti:LiNbO$_3$ optical strip waveguides for TE (*) and TM (o) polarizations versus the strip widths obtained by varying the temperature of the waveguide, the relative error being $\Delta\alpha/\alpha$ ~2.5 %. As may be seen from Fig. 3 the attenuation coefficient vs the waveguide width varies nearly linear in the range 5 µm ÷9 µm for both TE and TM, respectively polarizations.

As an example for a 7.5 µm wide X-cut waveguide we obtained α =0.78 dB/cm ($\Delta\alpha/\alpha$ =1.22%) and α =0.62 dB/cm ($\Delta\alpha/\alpha$ =1.43%) for TE and TM polarizations, respectively. The experimental errors of this method depend on the quality of the polished facets.
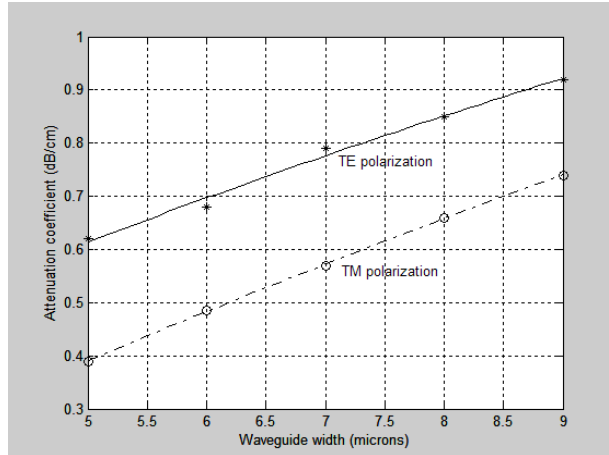

Fig. 3. Attenuation coefficient of X-cut Er^{3+}:Ti:LiNbO$_3$ optical strip waveguides for TE (*) and TM (o) polarizations versus the strip widths at λ = 1.5 μm.

2.2. Three prisms method for the measurements of the attenuation of low loss waveguides.

The most important feature quality waveguides is the level of the optical attenuation. One of the most effective ways of measuring the attenuation of light is the one using three prisms [14].
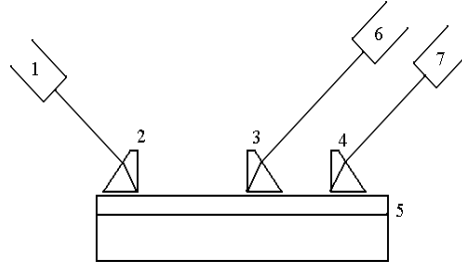

Fig. 4. Schematic layout of the three prisms methods of determining the optical losses: 1– laser, 2,3,4 – coupling prisms, 5 – waveguide, 6,7 –light intensity measuring photodiodes.

As shown in Fig. 4 prisms 2, 3 and 4 are couplet independently to the waveguide. Light intensity at the exit of prisms 3 and 4, when light enters through the 2, will be determined by the equations:

$$P_3 = \gamma_3 \cdot I(z_3) \tag{5}$$

$$P_4 = \gamma_4 [I(z_3) - P_3] \exp[-\alpha(z_4 - z_3)] \tag{6}$$

where P_3 and P_4 represent the output power of prisms 3 and 4; γ_3 , γ_4 - the unknown coupling constants of these prisms defining the light extraction intensity; $I(z$ $)$ - the light intensity in the waveguide at the distance z from the input prism 2; z_i is the location of the prism i; α is the attenuation coefficient of the waveguide.

For the two situations (with and without the prism 3) we will get:

$$I(z_3) \cdot (P_{40} - \Delta P) = (I(z_3) - P_3) \cdot P_{40} \tag{7}$$

$$I(z) = \frac{P_3 \cdot P_{40}}{\Delta P} \tag{8}$$

The result of this equation is independent of the coefficients $\gamma_2,$ γ_3 and γ_4 so that the light intensity can be calculated for the two positions A and B of the prism 3: z_{3A} and $z_{3B:}$

$$I(z_{3B}) = I(z_{3A}) \cdot \exp(-\alpha \cdot (z_{3B} - z_{3A})) \tag{9}$$

$$\alpha = \frac{\ln\left(\dfrac{P_{3A} \cdot \Delta P_B}{P_{3B} \cdot \Delta P_A}\right)}{z_{3A} - z_{3B}} \tag{10}$$

The resulting formula is independent of any of the coupling coefficients γ. For a precision by 3 % of light intensity the accuracy is estimated at 0.13 dB/cm.

Manufacture of planar multilayer waveguides with low losses were achieved by vacuum thermal evaporation at $(2 - 5) \cdot 10^{-6}$ Torr. The refractive index varies from 2.05 to 2.46 together with the decrease of the sulphur concentration from 95 % to 55 %. The optimal temperatures for the evaporator lay between 220 and 270 °C. The deposition process lasts $7 - 8$ minutes Fig. 5. The measurements of optical losses are presented in Table 1. The planar waveguides with low, less than 0.1 dB/cm was obtained.
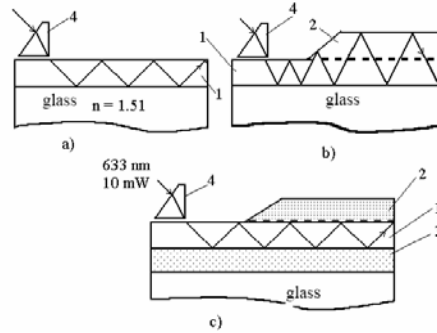

Fig. 5. Multilayer planar waveguides: 1– As_2S_3 , 2– As_2S_6 , 3 – As_2S_6 , 4–Coupling GaP prism.

Table 1.

Optical losses in planar waveguides for different As-S structure

Structure and composition	Sample no.	α [dB/cm] $\lambda = 0.63$ μm	α [dB/cm] $\lambda = 1.15$ μm
As_2S_3	1	3.0	1.4
	2	2.9	1.3
As_2S_5	1	1.8	Less than
	2	1.6	0.5
As_2S_6	1	1.6	Less than
	2	1.2	0.5
$As_2S_3+As_2S_6$	1	0.9	insignificant
$As_2S_6+As_2S_3+As_2S_6$	1	0.5	insignificant

3. Characterisation of the thin films refractive indexes

3.1. Determination of the refractive index profile from near field measurements

In this paper we present a method to determine the refractive index profile of a single mode waveguide from near field measurements [6-9]. The most important advantage of this method is that the waveguide is characterized at the operating wavelength with a non-destructive procedure; on the other hand the

disadvantage is that the near field measurements are affected by noise and errors due to the detection system and to the non-ideal focusing. This imposes the necessity to filter the field experimental data before the refractive index reconstruction.

In the scalar approximation using the theoretical models presented in papers [6,9] the refractive index profile, $n(x, y)$ may be determined from the scalar Helmholtz equation in the form:

$$n(x,y) \approx \left(\frac{\beta}{k_0}\right) - \frac{1}{2n_s k_0^2} \frac{\Delta_T \psi(x,y)}{\psi(x,y)} \tag{11}$$

where $\psi(x, y)$ is the transverse electric or magnetic field, β represents the propagation constant and k_0 is the vacuum wave vector.

Using the experimental arrangement presented in Fig. 6 we measured the near field intensity of an Er^{3+}:Ti:LiNbO$_3$ 7.5 μm width and 52 mm long X-cut waveguide. The measured field two-dimensional distribution (in the width and the depth of the waveguide) is presented in Fig. 7 a) while in Fig. 7 b) is presented the same distribution after the deconvolution procedure.
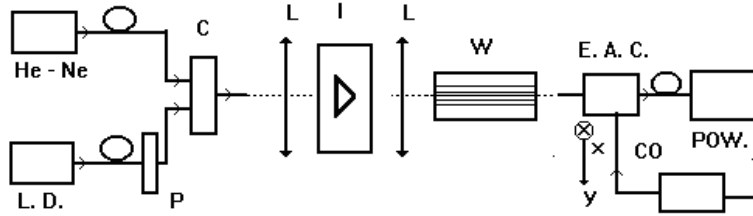

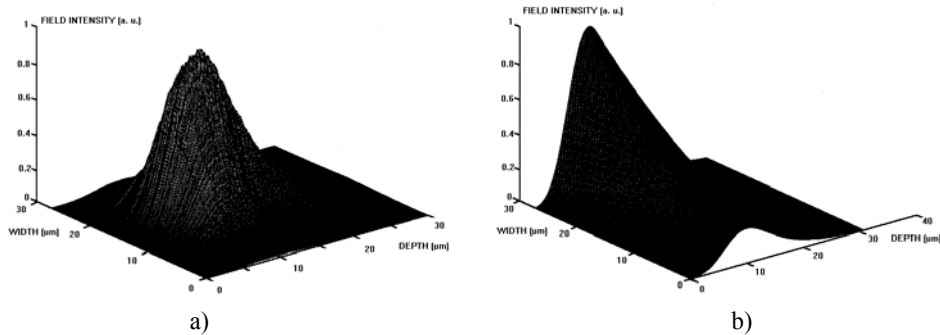Fig. 6. Schematic experimental setup for the near field measurement.

a)   b)

Fig. 7. a) The measured and **b)** deconvoluted field two-dimensional distribution

From the refractive-index profiles we obtained for the width refractive-index difference the value $\Delta n = 1.2 \cdot 10^{-3}$ and for the penetration depth $d_x = 3.5$ μm while in depth the corresponding values are $\Delta n = 1.08 \cdot 10^{-3}$ and $d_y = 6.5$ μm, respectively.
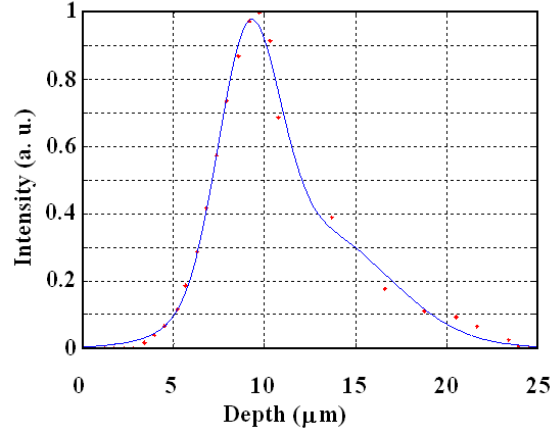

Fig. 8. The field profiles obtained using a 200x200 microns confocal microscopy;
the stars (*) are experimental data and the continuous curve (___) is
the fitted one with Gaussian functions.

The above mentioned results for the penetration depth in the depth of the waveguide are in good agreement with those obtained using a 200x200 microns confocal microscopy images (Fig. 8). In this case we obtained $d_y = 6.86$ μm.

3.2. Determination of the refractive index profile using holographic technique

To visualize the refractive index variation along a transversal section through an optical waveguide, we employ digital holographic microscopy technique which is a non-contact, non-invasive, marker free method to analyse transparent samples and which offers nanometric resolution in the axial direction. The lateral resolution is around 1 μm restricted by the diffraction limit, numerical aperture and magnification of the objective, dimensions of the recording sensor pixels, distances inside the experimental setup.

We use an experimental setup in the off-axis geometry based on the Mach-Zehnder interferometer, with the object placed in one arm. Two identical microscope objectives are inserted in both arms: in the object arm to magnify the sample details and in the reference arm to obtain the same curvature of the waves in the plane of the CCD camera sensor where are recorded the holograms. The used objectives have magnification of 40x which permits 0.9μm lateral resolution.

Two linear polarisers are used to ensure normal properties in the hologram plane recorded by the CCD (Pike F421 with Kodak sensor 2048x2048pixels, pixel pitch $\Delta x = 7.4\,\mu$m, acquisition rate of 16fps at full resolution). Starting from this pitch, we have chosen the minimum interfringe at $9\Delta x$, which corresponds to a spatial frequency of $1/(9\Delta x)$, which is in accordance with the maximum spatial frequency established by the Nyquist-Shannon sampling theorem of $1/(2\Delta x)$.

On the CCD camera sensor, we recorded the holograms formed through superposition between the reference and object wave; using a HeNe laser (double stabilized Spectra Physics). The last carries the diffracted filed from the object. In the hologram (see Fig. 9) we can see the specific maxima and minima of the diffraction pattern from waveguide edge and also the linear fringes from the interference pattern between object and reference wave. In Fig. 9 are some holograms obtained for waveguides with different dimensions in the transversal section (with square shape).

To reconstruct the object image, we use an algorithm based on the diffraction scalar theory in Fresnel approximation [15,16]. We follow the standard procedure [17] with steps which include: Fourier transform to separate the twin images, Fresnel transform to reconstruct the object image from the +1 order, correction for tilt and spherical aberrations, numerical focalization. In Fig. 9 are some images of the waveguides reconstructed from holograms. The main advantage of digital holographic microscopy technique is the fact that we record one single hologram from which we reconstruct the whole object, without mechanical scanning along propagation axis or in transversal plane. In Fig. 10 a) and b) are 2D images in false colours or in gray levels which are calibrated in values of the phase shift introduced by the sample in the optical path.

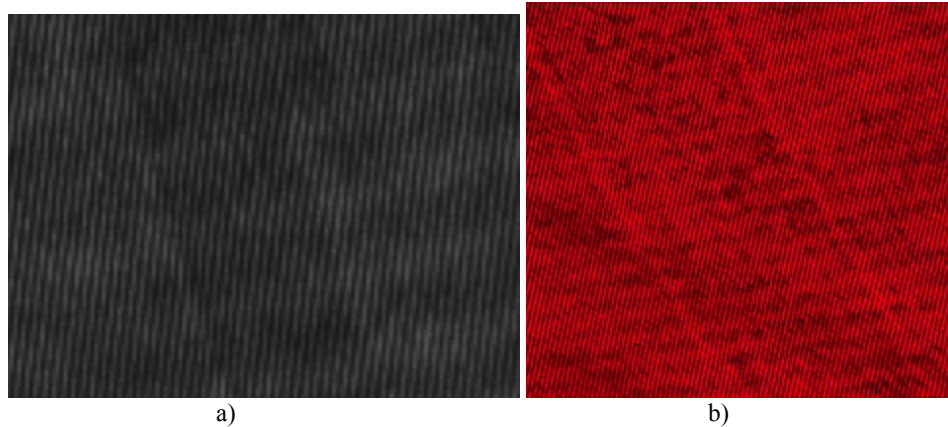a)   b)
Fig. 9. Holograms recorded experimentally for two waveguides with different widths.

In Fig. 10 c) and d) are 3D representations of the same waveguides and on the third axis are also values for the phase shift. The dimension calibrations in the transversal plane were done using an object made with electron beam lithography, with precise dimensions.

a)   b)   c)   d)
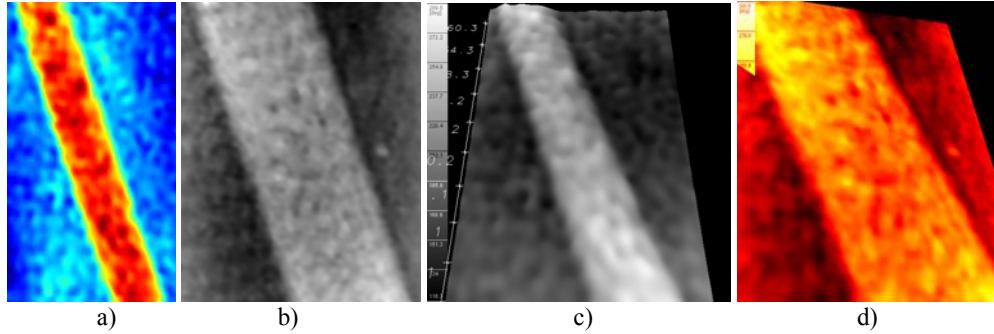
Fig. 10 a) - d). The reconstructed images of two waveguides.

In these investigations using digital holographic microscopy technique, we have quantitative information along the propagation axis, about the phase shift introduced by the object in the optical path proportional with the geometrical height and with the difference between refractive indices of the waveguide and of the surrounding medium:

$$\Delta\Phi = \frac{2\pi}{\lambda} h_w (n_w - n_{sm}) \tag{12}$$

where λ is the wavelength of the He-Ne laser 632.8 nm, h_w is the geometrical height of the waveguide, n_w and n_{sm} are the refractive indices of the waveguide and of the surrounding medium, respectively.
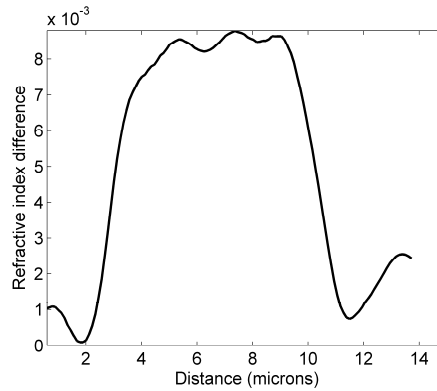

Fig. 11. Profiles for the waveguides refractive index (the difference between values of the waveguide and of the surrounding medium, respectively).

From the phase shift introduced by the sample, we calculate its refractive index profile, when we suppose that its transversal section is square. In the case of these waveguides, we know the refractive index of the surrounding material LiNbO₃ n_{sm}=2.28646 at 632.8 nm. The values resulted for the profile of refractive index difference $n_w - n_{sm}$ is shown in Fig. 11.

3.3. Refractive index characterization of As₂S₃ films. Establish of the optical anisotropy

The two prisms method measurements (fig. 12) was used to characterise the refractive index in case of waveguides with step distribution, like amorphous As₂S₃ thin films obtained by thermal vacuum deposition. In this method the light propagates along the dielectric layer, but only some values of the incidence angle form an electromagnetic field with certain configurations. This method is known as m-line spectroscopy.
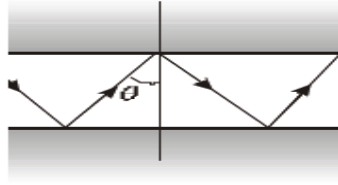

Fig. 12. Light propagation in planar waveguides. Geometrical approximation.

Vitreous As₂S₃ thin films were made with thicknesses in the range from 0.7 µm to 4.5 µm. The results of the measurements are presented in Table 2.

Table 2

The measured exit angles toward the prism normal

Mode number	Exit angles for TE mode	Exit angles for TM mode
0	31.013	30.511
1	28.441	27.741
2	23.997	22.844
3	18.326	16.671
4	11.182	8.864

By this method we obtained only refractive index and film thickness, but to enhance the accuracy we used an optimization algorithm as: for each mode pairs the computer calculates an average of the refractive index and the thickness of the layer. Subsequently standard deviations are calculated and the results are

optimized using the least squares method. The results of this data processing are displayed in Table 3.

Anisotropy of amorphous As$_2$S$_3$ films at the wavelength of 0.63 μm

Sample number	Film thickness	Refractive index normal toward the film plane n_{fn}	Refractive index in the film plane n_{fp}	Index anisotropy δn	Standard deviation
1	0.71	2.413	2.393	0.020	0.001
2	1.58	2.403	2.385	0.018	0.0009
3	2.97	2.405	2.397	0.008	0.0008
4	4.20	2.407	2.401	0.006	0.0006
5	4.50	2.406	2.402	0.004	0.0008
1A	0.70	2.426	2.414	0.012	0.002

These results led to the fact that the refractive index anisotropy can reach the level of 0.020 in the case of thin films. A conclusion of these results is that the amorphous chalcogenide compounds have two typical aspects: the photoelasticity phenomenon is very pregnant in these materials and the explanation for the modifications that appear due to the illumination frames to the phenomenon of photoinduced fluidity .

3.4. Characterization of the refractive index dispersion of As$_2$S$_3$ films

Using a new simple method the films refractive index the dispersion curve of the refractive index and the modification of the dispersion curve $n(\lambda)$ in As$_2$S$_3$ thin films as a result of the Argon laser irradiation was measured and investigated over a wide spectral range. This method [18] involves calculating the transmission and reflection of light of the structure (AIR-FILM-SUBSTRATE-AIR). Optical absorption was ignored in the development of the formulae. The calculations will be done taking into account the following: in spectral devices used for such kind of measurements, the beam which illuminate the structure is obtained by white light decomposition in a monochromator; interference fringes can be definitely noticed in films thinner than 10 μm, for a monochromator resolution of 1-10 nm; interference doesn't appear in substrates having a real thicknesses of 2-3 mm.

$$n_S = \frac{1+\sqrt{1-T_o^2}}{T_o} \tag{13}$$

$$n_f = \sqrt{N \pm \sqrt{N^2 - n_S^2}} \tag{14}$$

$$N = \frac{2n_S}{T_1} - \frac{n_S^2+1}{2} \tag{15}$$

For the investigation the films were deposed on a polished and well cleaned glass substrate in order to diminish the light scattering and the intensity was of 20 – 40 mW/cm^2. Using the expression (15) with the sign plus the refraction index of the film is calculated starting from the measured transmission values in minima. The refractive index was measured in the spectral range 0.6 – 1.0 μm. The dispersion curves are displayed in Fig.13. for various intensities and an exposure time of 60 s.

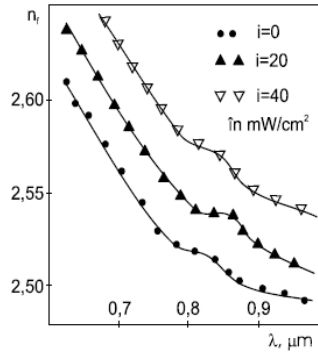
Fig. 13. Spectral dependence of the refractive index of the amorphous As$_2$S$_3$ films and the modifications induced by a laser beam illumination

It can be seen that illumination produces considerable increases of the refractive index in the whole spectral range and in the short waves domain the variation of the refractive index Δn = 0.07 is larger than in the larger wavelengths spectral domain (λ=1.0 μm), where it increases with 0.04 only. Due to a higher density of the energetic states was noticed a larger increase of the refractive index in the waveband of 0.85 μm.
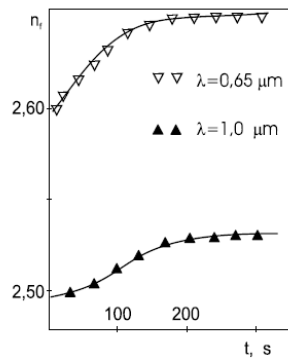

Fig. 14. Refractive index modifications in As$_2$S$_3$ films for two spectral domains.

In Fig. 14 are presented the character of the refractive index evolution in time is distinct for different spectral bands. An increase of the refractive index

when increasing the illumination is observed at the wavelength of 0.65 μm. In the long waves spectral band of $\lambda=1.0$ μm a delay is noticed, a retention in time, and only after 50-60 s the refractive index begins to increase.

4. Absorption and emission cross sections spectra

The exact knowledge of the absorption and emission cross sections of the rare earth doped $LiNbO_3$ optical waveguides is required in the theoretical modelling of the guided lasers and amplifiers.

Based on the density matrix formalism and the Mc Cumber's theory authors of [6, 20] analyse the homogeneous absorption and emission cross sections may be determined from the experimental (inhomogeneous) cross sections $\sigma_a^I(\lambda)$ through the inverse Fourier transform relation (and its properties). The experimental spectra (Fig. 15) may be numerically fitted with the following equation [6,20]:

$$I(\lambda) = \sum_i a_i \exp\left[-4\log 2 \frac{(\lambda - \lambda_i)^2}{\Delta\lambda_i^2}\right]. \qquad (16)$$

The inhomogeneous absorption (a) and emission (e) cross sections $\sigma_{a,e}^I(\omega)$ are proportional to the experimental line shape $I_{a,e}(\lambda)$. The homogenous absorption and emission cross section $\sigma_{a,e}^H(\omega)$ may be determined from the experimental inhomogeneous cross sections by inverse Fourier transformation as:

$$\sigma_{a,e}^H(\omega) = F^{-1}\left[\exp\left(\frac{\Delta\omega_{inh}x^2}{16\log 2}F\left[\sigma_{a,e}^I(\omega);x\right]\omega\right)\right], \qquad (17)$$

where $\Delta\omega_{inh} = 2\pi c\Delta\lambda_{inh}/\lambda^2$ is the inhomogeneous bandwidth and $\Delta\lambda_{inh}$ the inhomogeneous line width. The fitting curve is not unique but the deconvolution expressed in $\sigma_{a,e}^H(\omega)$ has a unique solution. Once we have obtained the absorption cross section, the emission cross section may be obtained using the relation [6]:

$$\sigma_e(\nu) = \sigma_a(\nu)\exp\left[\frac{h(\nu - \varepsilon)}{k_B T}\right], \qquad (18)$$

where:
$$h\varepsilon \cong -k_B T\log(N_2/N_1), \qquad (19)$$

$N_{1,2}$ being the populations of the two-level system Stark splitted implied in transitions and ε the excitation energy.
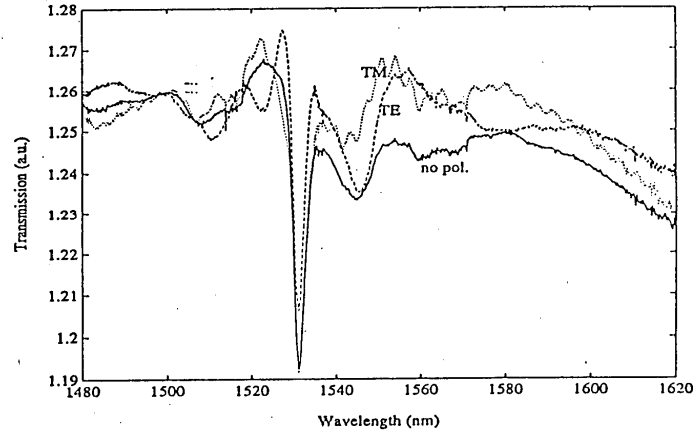
Fig. 15. The transmission spectra of a 7.5 μm Er^{3+}:Ti:LiNbO$_3$ optical waveguide in the range 1480-1620 nm. a) without polarization, b) TE and c) TM, respectively polarizations.

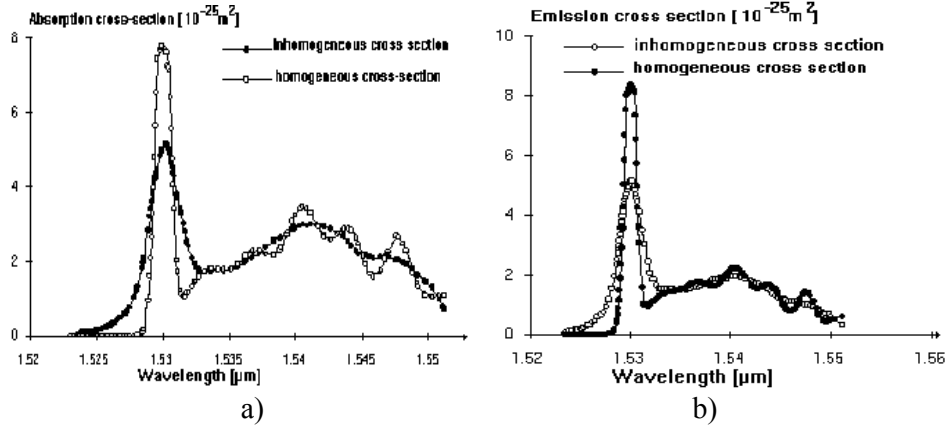a)   b)

Fig. 16. a) The unpolarised inhomogeneous and homogeneous absorption and
b) emission cross section spectra of an Er^{3+}:Ti:LiNbO$_3$ waveguide.

Using a laser amplifier as signal source, (Fig. 1) different absorption bands have been investigated in the range 1480-1620 nm. In Fig. 15 are presented the measured transmission spectra of a 7.5 μm Er:Ti:LiNbO$_3$ waveguide for the unpolarised case and for both TE and TM polarizations. The most significant peak in the absorption spectra is located around 1532 nm and corresponds to the transition $^4I_{15/2} \rightarrow ^4I_{13/2}$. Then by using the theoretic model presented in papers [6, 19] we evaluated the unpolarised homogeneous absorption and emission cross sections (Fig. 16 a), b)) obtaining the peak values 1.3×10^{-24} m^2

and 1.8×10^{-24} m^2, respectively. For the simulation of the inhomogenious absorption spectra we used eight Gaussian functions to assure the best fit with the experimental data.

5. Conclusions

The measurements of optical losses (attenuation), refractive index and absorption/emission spectra for the characterization of Er^{3+}: doped Ti in-diffused LiNbO$_3$ and amorphous As$_2$S$_3$ chalcogenide waveguides are provided using non-destructive optical methods.

The waveguide losses have been measured by the low finesse resonator method, the absorption spectra have been deduced by subtraction of the measured waveguide transmitted spectra of doped and un-doped waveguides; the near field profile has been measured scanning the waveguide transversal section through a fibre probe. The measured data have been numerically deconvoluted with a Gaussian-like function that approximates the fibre field profile. The near field profile has been used to obtain the refractive index distribution in depth and width while the absorption spectra have been assumed as the starting point for the evaluation of the homogenous absorption and emission cross sections. Calculations obtained from numerical simulations performed by varying the refractive index shows that symmetrical waveguides with low refractive index difference are less sensitive to disorder.

For the waveguides with step refractive index distribution prism coupling method can be used. Due to bad reproducibility of coupling coefficient, three prisms method need to be used to provide measurements of low losses. The accuracy of the refractive index characterisation by m-line spectroscopy permits the establish of optical anisotropy for amorphous As$_2$S$_3$ films obtained by thermal vacuum deposition.

Acknowlegments

R E F E R E N C E S

[1] *H. Hu, R. Ricken, and W. Sohler*, "Etching of lithium niobate: micro- and nanometer structures for integrated optics", Topical Meeting "Photorefractive Materials, Effects, and Devices – Control of Light and Matter, Bad Honnef, June, 2009.

[2] *M. García Granda, H. Hu, W. Sohler, and J. Rodríguez García,* "Novel structures for broadband electrooptic modulators in $LiNbO_3$", Proc. 14th European Conference on Integrated Optics (ECIO`08), Eindhoven, Netherlands, paper WeD4, p. 79-82, 2008.

[3] *E. Saglamyurek, N. Sinclair, J. Jin, J. A. Slater, D. Oblak, F. Bussières, M. George, R. Ricken, W. Sohler and W. Tittel,* "Broadband waveguide quantum memory for entangled photons", (invited), 2011 IEEE Photonics Society Summer Topical Meeting, Montreal, Canada, 18 - 20 Jul., 2011.

[4] *M. Kawai, K. Mori,* "Optical components and devices for next-generation photonic networks", FUJITSU Sci. Tech. J. Vol. 42**,** No. 4, p. 483-493, 2006.

[5] *W. Sohler, B. Das, D. Dey, S. Reza, H. Suche, and R. Ricken*, Erbium-doped lithium niobate waveguide lasers, (invited paper), IEICE Transactions Electron E, Vol. 88-C, No. 5, p. 990-997, 2005.

[6] *N. N. Puscas, D. M. Grobnic, I. M. Popescu, M. Guidi, D. Scarano, G. Perrone, I. Montrosset,* "Characterization of the Er^{3+}-Doped $Ti:LiNbO_3$ Waveguides: Losses, Absorption Spectra and Near Field Measurements", Optical Engineering, Vol**.** 35**,** No. 5, p. 1311-1318, 1996.

[7] *A. Popescu, S. Miclos, D. Savastru, R. Savastru, M. Ciobanu, M. Popescu, A. Lőrinczi, F. Sava, A. Velea, F. Jipa, M. Zamfirescu,* "Direct laser writing of two-dimensional photonic structures in amorphous As_2S_3 thin film", J. Optoelectron. Adv. Mater., vol. 11, No. 11, p. 1874 – 1880, 2009.

[8] *M. Popescu, A. Velea, A. Lőrinczi, M. Zamfirescu, F. Jipa, S. Miclos, A. Popescu, D. Savastru*, Dig. J. Nanomater. Bios., **5**(4), 1579 (2010).

[9] *J. Helms, Joachim Schmidtchen, B. Schuppert and K. Peterman*, "Error Analysis for Refractive-Index Profile Determination from Near-Field Measurements", Journal of Lightwave Tehnology*,* Vol. LT- 8, p. 625-634, 1990.

[10] *E. M. Vogel, M. J. Weber, D. M. Krol*, Physics and Chemistry of Glasses**,** 32**,** 231 (1991).

[11] *Lenz, J. Zimmermann, T. Katsufuji, M. E. Lines, H. Y. Hwang, S. Spalter, R. E. Slusher, S. W. Cheong, J. S. Sanghera, I. D. Aggarwal*, Opt. Lett., 25, 254 (2000).

[12] R. Regener W. Sohler, "Loss in Low- Finesse $Ti:LiNbO_3$ Optical Waveguide Rezonator"; Appl.Phys., Vol. B 36, p. 143-147, (1985).

[13] *Y. H. Won, P. C. Jaussaud, G. H. Chartier*, Appl. Phys. Lett., 37, 269 (1980).

[14] *A. A. Popescu[*], D. Savastru, S. Miclos,* "Design and realization of low losses chalcogenide As_xS_{1-x} planar waveguides", Journal Of Optoelectronics And Advanced Materials, Vol. 13, No. 3, p. 213 – 217, March 2011.

[15] *T. Montfort, F. Charrière, T. Colomb, E. Cuche, P. Marquet, C. Depeursinge*, "Purely numerical compensation for microscope objective phase curvature in digital holographic microscopy: influence of digital phase masks position", J. Opt. Soc. Am. A 23, p. 2944-2953, 2006.

[16] *Tristan Colomb, Nicolas Pavillon, Jonas Kühn, Etienne Cuche, Christian Depeursinge, and Yves Emery*, "Extended depth-of-focus by digital holographic microscopy", Optics Letters, Vol. 35, Issue 11, 2010, pp. 1840-1842.

[17] http://www.lynceetec.com/content/view/497/193/

[18] *A. Popescu, D. Savastru, S. Miclos*, „Refractive index anisotropy in non-crystalline As_2S_3 films", Journal Of Optoelectronics And Advanced Materials, **Vol. 12**, No. 5, P.1012 – 1018, May 2010.

[19] *A. Popescu,* „Photo-induced phenomena and integrated optical elements based on non-crystalline chalcogenide semiconductors", Stiinta, Chisinau 2003.

[20] *E. Desurvire,* "Erbium-Doped Fiber Amplifiers"*,* J. Wiley & Sons, Inc. New York, 1994.